


Article

Study on Electrochemical Properties of Carbon Submicron Fibers Loaded with Cobalt-Ferro Alloy and Compounds

Peilong Xu ¹, Qinghui Yuan ², Wendong Ji ², Yuling Zhao ¹, Ruitao Yu ³, Yimin Su ⁴ and Ningbo Huo ^{2,*}

¹ State Key Laboratory of Bio-Fibers and Eco Textiles, Qingdao University, No.308 Ningxia Road, Qingdao 266071, China

² Binzhou Polytechnic, No.919 Huanghe 12th Road, Binzhou 256600, China

³ College of Electronics and Information, Qingdao University, No.308 Ningxia Road, Qingdao 266071, China

⁴ College of Art and Design, Beijing University of Technology, 100 Pingleyuan, Chaoyang District, Beijing 100124, China

* Correspondence: huoningbo@bzpt.edu.cn

Abstract: In this work, carbon submicron fiber composites loaded with a cobalt-ferric alloy and cobalt-ferric binary metal compounds were prepared by electrospinning and high temperature annealing using cobalt-ferric acetone and ferric acetone as precursors and polyacrylonitrile as a carbon source. The phase transformation mechanism of the carbon submicron fiber-supported Co-Fe bimetallic compound during high temperature annealing was investigated. The electrochemical properties of the carbon submicron fiber-supported Co-Fe alloy and Co-Fe oxide self-supported electrode materials were investigated. The results show that at 138 °C, the heterogeneous submicron fibers of cobalt acetylacetonate and acetylacetonate iron began to decompose and at 200 °C, CoFe₂O₄ was generated in the fiber. As the annealing temperature increases further, some metal compounds in the carbon fiber are reduced to CoFe₂O₄ alloy, and two phases of CoFe₂O₄ and CoFe-Fe-alloy exist in the fiber. After 200 cycles, the specific capacity of CF-P500 is 500 mAh g⁻¹. The specific capacity of the composite carbon submicron fiber electrode material can be significantly improved by the introduction of CoFe₂O₄. When the binary metal oxides are used as electrode materials for lithium-ion batteries, alloy dealloying and conversion reactions can occur at the same time in the reverse process of lithium intercalation, the two reactions form a synergistic effect, and the cobalt-iron alloy in the material increases the electrical conductivity. Therefore, the carbon submicron fiber loaded with CoFe₂O₄/CoFe has an excellent electrochemical performance.

Keywords: carbon submicron fiber composites; loaded with cobalt-ferric alloy; cobalt-ferric binary metal compounds; electrochemical performance



Citation: Xu, P.; Yuan, Q.; Ji, W.; Zhao, Y.; Yu, R.; Su, Y.; Huo, N. Study on Electrochemical Properties of Carbon Submicron Fibers Loaded with Cobalt-Ferro Alloy and Compounds. *Crystals* **2023**, *13*, 282. <https://doi.org/10.3390/cryst13020282>

Academic Editors: Dongjie Zhang, Qixing Xia, Qiang Tao, Haiyang Zhang and Dmitry Medvedev

Received: 10 January 2023

Revised: 25 January 2023

Accepted: 3 February 2023

Published: 7 February 2023



Copyright: © 2023 by the authors. Licensee MDPI, Basel, Switzerland. This article is an open access article distributed under the terms and conditions of the Creative Commons Attribution (CC BY) license (<https://creativecommons.org/licenses/by/4.0/>).

1. Introduction

In the research of materials in the field of energy storage, the synergistic effect between different metal components of alloys and binary metal compounds can significantly improve the electrical conductivity and electrochemical activity of materials, which is more favored than single metals and their compounds. The theoretical specific capacity of binary metal oxides is higher than that of single metal oxides, the reaction process is highly complementary, and the binary metal oxides have obvious advantages over single metal oxides; thus, the research potential is huge [1–8]. The general formula of binary metal oxide molecules is A_xB_{3–x}O₄, where A and B are usually two of Fe, Co, Ni, Zn or other elements. The commonly reported binary metal oxides are ferrates (e.g., CoFe₂O₄ [9] and NiFe₂O₄ [10]), cobaltates (e.g., NiCo₂O₄ [11] and ZnCo₂O₄ [12]) and manganate (e.g., CoMn₂O₄ [13] and NiMn₂O₄ [14]). When these oxides are used as electrode materials for lithium ion batteries, alloying/dealloying and conversion reactions can occur simultaneously in the reverse process of lithium insertion/demineralization, and the two reactions form a synergistic effect, resulting in a better lithium storage capacity [15–18].

As electrode materials, although binary metal oxides have excellent lithium storage capacity, they also have the disadvantage of a poor cycling stability caused by volume expansion and crushing [19]. In order to further improve the conductivity and stability of binary metal oxides, research on their composites with carbon materials has attracted wide attention. Xie et al. [20] used a CoFe_2O_4 composite MXene thin film to prepare high-performance flexible materials for flexible supercapacitors, showing good cyclic performance. Wu et al. [21] used polyaniline as a precursor to synthesize iron/cobalt compound-/carbon-based composite materials at high annealing temperatures as a catalyst for fuel cells. Some metal compounds easily form an alloy phase with other metals at high temperatures. For example, cobalt compounds easily form alloys with chromium, tungsten, iron, nickel and so on at high temperature reduction states. Ji et al. [22] prepared cobalt-iron/biomass porous carbon (CoFe/BPC) composite materials using Chinese fir as a raw material by an in situ reduction process, which have excellent electromagnetic wave absorption performance due to their graphitization, porous structure, strong magnetism and multi-component effect.

Although remarkable progress has been made in the electrochemical research of binary metal oxide/carbon submicron fiber composites, the study of the phase transition mechanism in the preparation process is still insufficient. Elucidating the phase transition process can provide new ideas for the preparation of different bimetallic compound-doped carbon matrix composites, which has important practical value.

In this work, carbon submicron fiber composites loaded with cobalt-ferric alloys and cobalt-ferric binary metal compounds were prepared by electrospinning and high temperature annealing using cobalt-ferric acetone and ferric acetone as precursors and polyacrylonitrile as the carbon source. The phase transformation mechanism of carbon submicron fiber supported Co-Fe bimetallic compounds during high temperature annealing was investigated. The electrochemical properties of carbon submicron fiber supported Co-Fe alloys and Co-Fe oxide self-supported electrode materials were investigated.

2. Experimental

2.1. Preparation of Carbon Submicron Fiber Films Loaded with Cobalt-Ferric Alloy and Cobalt-Ferric Oxide

An amount of 1.426 g polyacrylonitrile (PAN), 0.67 g iron acetylacetonate $\text{C}_{15}\text{H}_{24}\text{FeO}_6$ ($\text{Fe}(\text{acac})_3$) and 0.34 g cobalt acetylacetonate $\text{C}_{15}\text{H}_{21}\text{CoO}_6$ ($\text{Co}(\text{acac})_2$) (molar ratio Fe:Co = 2:1) were added to 10 mL of dimethylformamide (DMF), the PAN content was 12 wt.%. A mixed spinning solution was obtained by stirring at room temperature for 2 h with the content of 8.5 wt.%. An appropriate amount of the solution was extracted with a 5 mL syringe and fixed on the propulsion pump. At the temperature of 26 °C, humidity of $36 \pm 2.5\%$ and static electric field voltage of 20 kV, silk spraying was performed at the speed of 0.36 mL/h to form a film. The film was placed in a drying oven at 30 °C for 2 h, and a heterogeneous submicron fiber film loaded with cobalt acetyl acetone/iron was obtained, labeled as CF-P 25. The sample CF-P 25 was heated to 230 °C in an air atmosphere and kept at a constant temperature for 2 h to preheat and stabilize. Then, the sample was obtained by natural lowering to room temperature and labeled as CF-P 230. The pre-heated stabilized samples were moved into a tube furnace and heated to 400 °C, 500 °C, 600 °C, 700 °C and 800 °C, respectively, at a heating rate of 2 °C/min under the protection of argon gas. After constant temperature heating for 2 h, the samples of the carbon submicron fiber films loaded with a cobalt-ferro alloy and its compounds were obtained at different annealing temperatures. They were named CF-P 400, CF-P 500, CF-P 600, CF-P 700 and CF-P 800.

2.2. Preparation of Lithium-Ion Batteries

The electrolyte was 1 M LiPF_6 (1:1 volume ratio of carbonate/dimethyl carbonate), and lithium metal sheet was used as the counter electrode. A CR2025 button battery was assembled in a glove compartment filled with high purity argon (moisture and oxygen concentration less than 0.1 ppm). CF-P 500 and CF-P 600 could be directly used as self-

supporting anode materials for lithium-ion batteries without adding additional binders or conductive additives such as carbon black.

2.3. Method

In order to study the phase transitions of compounds in the heterogeneous fibers during annealing, firstly, CF-P 400, CF-P 500, CF-P 600, CF-P 700 and CF-P 800 were characterized by SEM and XRD. The optimum annealing temperature was found and the mechanism of phase transformation was further studied by means of TGA and TEM. Finally, in the material characterization section, an electrochemical workstation was used for analysis using a two-electrode setup. Cyclic voltammetry (CV) curves and electrochemical impedance spectroscopy (EIS) curves were measured.

The models of instruments used in the experiment were SEM: JEOL JSM-6390LV; XRD: BRUKER D8 Advance; TEM: JEOL JEM2100F; TGA: NETZSCH TG 209; and electrochemical workstation: Parstat MC.

The Analysis and Testing Center of Qingdao University provided technical support for these experiments.

3. Results and Discussion

Submicron Fiber Structure and Annealing Phase Transformation Mechanism of Loaded Binary Metal Compounds

The heterogeneous submicron fibers loaded with cobalt-iron binary metals and their compounds were characterized by scanning electron microscopy (SEM). Figure 1a,c,e,g and Figure 2a,c,e are low-magnification and high-magnification SEM images of the heterogeneous submicron fiber CF-P 25-800, respectively. In the low magnification image, the fiber diameter is uniform, the surface is smooth, there are no nodules or beading phenomenon, no adhesion between the cross fibers and the fiber diameter decreases gradually with the increase in annealing temperature. Figure 1b,d,f,h and Figure 2b,d,f are SEM images of a single fiber. It can be observed from Figure 1b that there is a small concave-convex morphology on the fiber surface. Figure 1d shows the surface topography of a single fiber of CF-P 230 after preheating and stabilizing at 230 °C in air. As can be seen from the figure, after preheating and stabilizing, the concave-convex condition of the fiber surface was significantly enhanced, indicating that the material in the heterogeneous submicron fiber at this temperature has thermal dynamic motion. Figure 1f,h shows the surface topography of single fibers in CF-P 400 and CF-P 500 annealed at 400 °C and 500 °C. It can be seen that the fiber surface not only has concavity, but also has begun to form a strip morphology. Figure 2b shows the surface topography of a single fiber in the sample CF-P 600 annealed at 600 °C. The banded morphology of the fiber surface in the figure is more obvious than that of the fiber surface in CF-P 500.

When the annealing temperature was 700 °C, the strip on the fiber surface was more obvious and depressions were formed by the shedding of surface materials, as shown in Figure 2d. This indicates that at the annealing temperature of 700 °C, carbon submicron fibers form on the substances attached to the surface. Figure 2f shows the surface morphology of a single fiber in sample CF-P 800 at an annealing temperature of 800 °C, which is similar to that of CF-P 700. The fiber surface not only presents obvious banding, but also has more obvious depression formed by material shedding. A similar phenomenon was observed on the surface of heterogeneous carbon submicron fibers loaded with cobalt and its compounds and on the surface of carbon fibers loaded with iron compounds. It was shown that the compounds move from the interior of carbon fibers to the surface with the increase in annealing temperature during the preparation of these compounds. Using this phenomenon, the composition of heterogeneous carbon submicron fibers can be designed by controlling the annealing process.

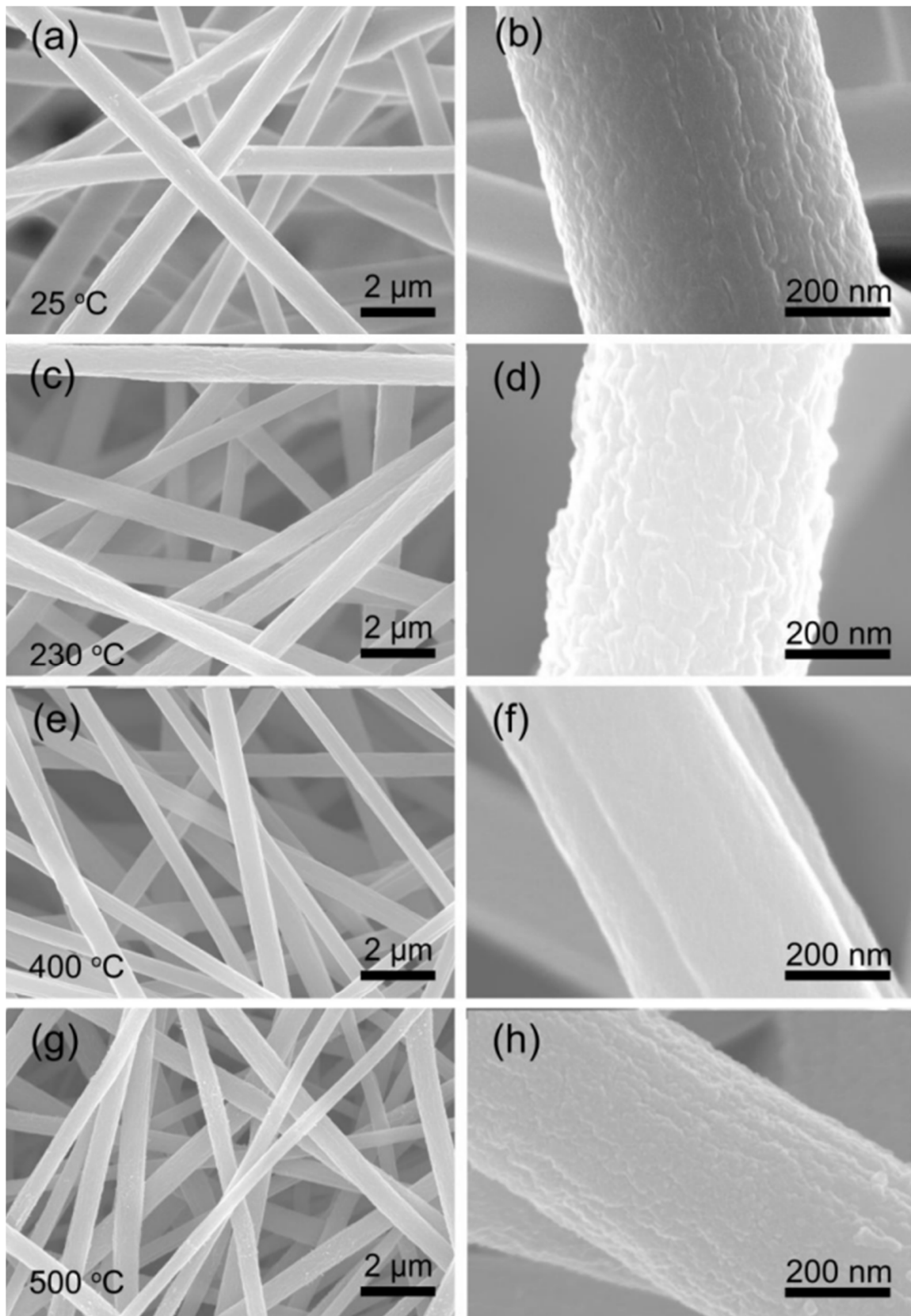


Figure 1. Low magnification and high magnification SEM images of heterogeneous submicron fibers loaded with binary metals and their compounds: ((a,b), 25 °C) CF-P25, ((c,d), 230 °C) CF-P 230, ((e,f), 400 °C) CF-P 400, ((g,h), 500 °C) CF-P 500 samples.

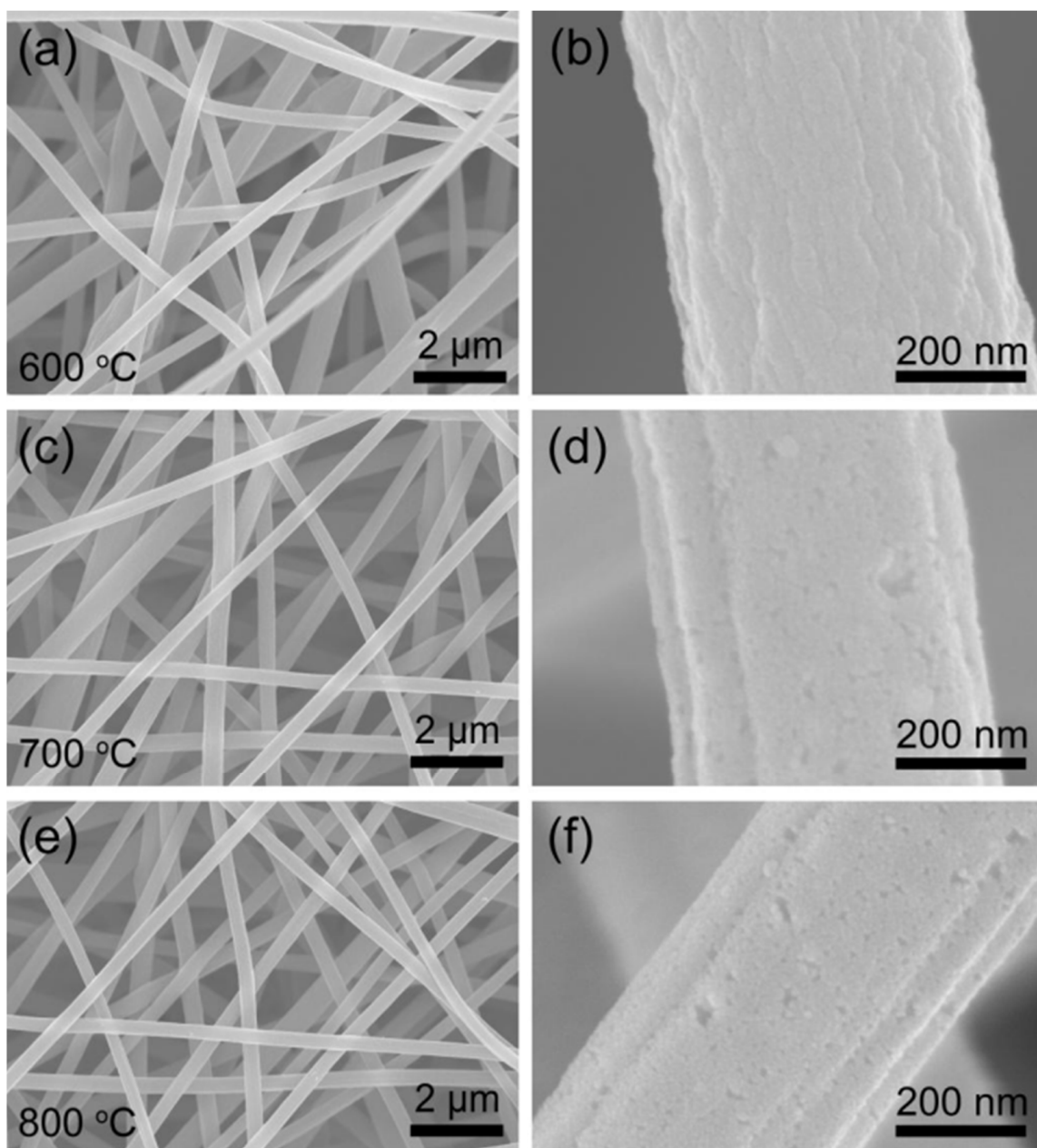


Figure 2. Low magnification and high magnification SEM images of heterogeneous submicron fibers loaded with binary metals and their compounds: ((a,b), 600 °C) CF-P 600, ((c,d), 700 °C) CF-P 700, ((e,f), 800 °C) CF-P 800.

In order to investigate the phase changes of compounds in heterogeneous fibers during annealing, the heterogeneous submicron fibers loaded with binary metals and their compounds at different annealing temperatures were characterized by XRD. Figure 3 shows the XRD patterns of the samples CF-400, CF-500, CF-600, CF-700 and CF-800. For the sample annealed at 400 °C, there is a weak diffraction peak at 44.9°. When the temperature rises to 500 °C, the diffraction peak at 44.9° is significantly enhanced and a diffraction peak begins to appear at 65.3°. The two diffraction peaks correspond to (110) and (200) crystal plane diffraction peaks of cubic phase cobalt-ferro alloy CoFe (JCPDS no.: 44-1433), respectively. With the increase in annealing temperature, the diffraction peak of the cobalt-ferro alloy becomes more sharp, indicating that cobalt-ferro oxide is reduced to cobalt-ferro alloy by the carbon in the carbon fiber with the increase in annealing temperature. In the XRD patterns of CF-P 600, CF-P 700 and CF-P 800, only the characteristic diffraction

peaks of cubic phase cobalt-ferro alloys exist. The above results show that cobalt and iron oxides are formed in the fibers under 400 °C. With the increase in annealing temperature, some cobalt-iron oxides are reduced to cobalt-iron alloys by carbon. When the annealing temperature rises above 600 °C, cobalt iron oxide is reduced to cobalt iron alloy by the carbon in the carbon fiber.

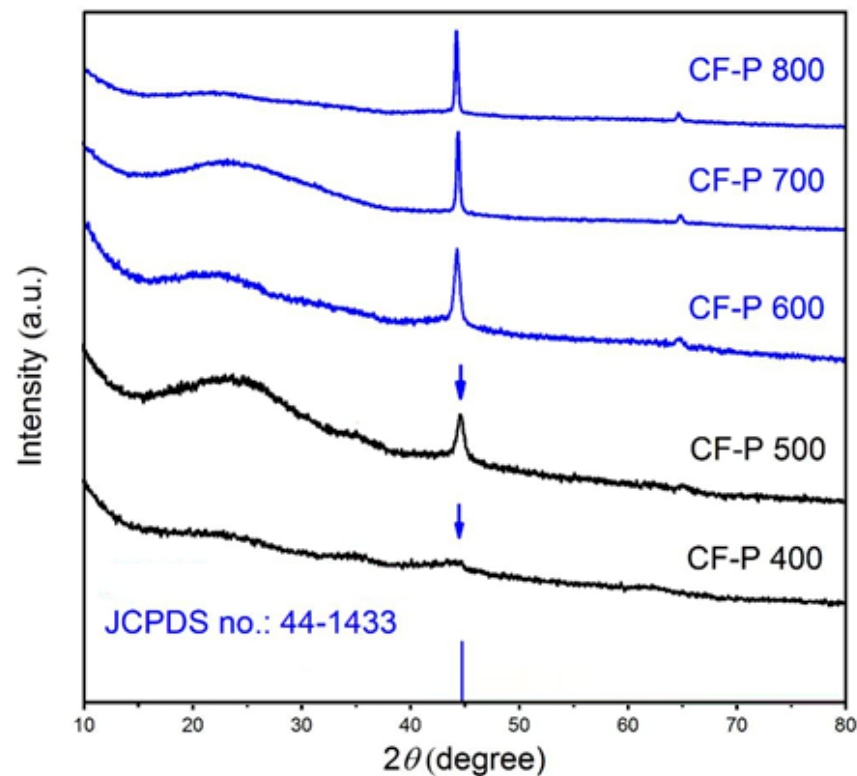


Figure 3. XRD patterns of samples CF-400, CF-500, CF-600, CF-700 and CF-800. The area of the XRD peak indicates the crystal content; the larger the area, the higher the crystal phase content. A narrow peak indicates a large grain size, which can be calculated by Scherrer's formula. The XRD pattern peak is high if the relative background strength is high, indicating a high crystal phase content, consistent with the area indicating the crystal phase content [23].

In order to further determine the specific phase transition characteristics of cobalt-iron compounds in heterogeneous fibers with the increase in annealing temperature, transmission electron microscopy was used to characterize the microstructure of CF-P 500 and CF-P 600, as shown in Figure 4. It can be seen from the low magnification morphologic image of the fiber that small particles are distributed on the surface of the fiber (Figure 4a,c). The HRTEM images of samples CF-P 500 and CF-P 600 were measured, and it was found that in the HRTEM images of sample CF-P 500 annealed at 500 °C, as shown in Figure 4b, in the nanocrystalline grains marked by the green dotted line, the spacing between two crystal surfaces was 2.53 Å. An angle of 129° corresponds to the cubic crystal phase CoFe_2O_4 (311) surface and (3) face. The red arrows in Figure 3 indicate the diffraction peak characteristic of CoFe_2O_4 . The yellow dotted line marks a grain spacing of 2.04 Å, corresponding to the cubic phase of CoFe (110) and (1, 1) in CF-P 500 CoFe_2O_4 . Cobalt and iron in the two phases are coexistent. The HRTEM CF-P 600 is shown in Figure 4d, with an interplanar spacing of 2.02 Å, two crystal angle of 90° corresponding to the CoFe (110) surface and (1, 1), respectively. A large number of HRTEM analyses showed that only a CoFe_2O_4 phase was found in the sample CF-P 600, which is consistent with the XRD results, indicating that CoFe_2O_4 has been completely reduced to the CoFe-Fe alloy at the annealing temperature of 600 °C.

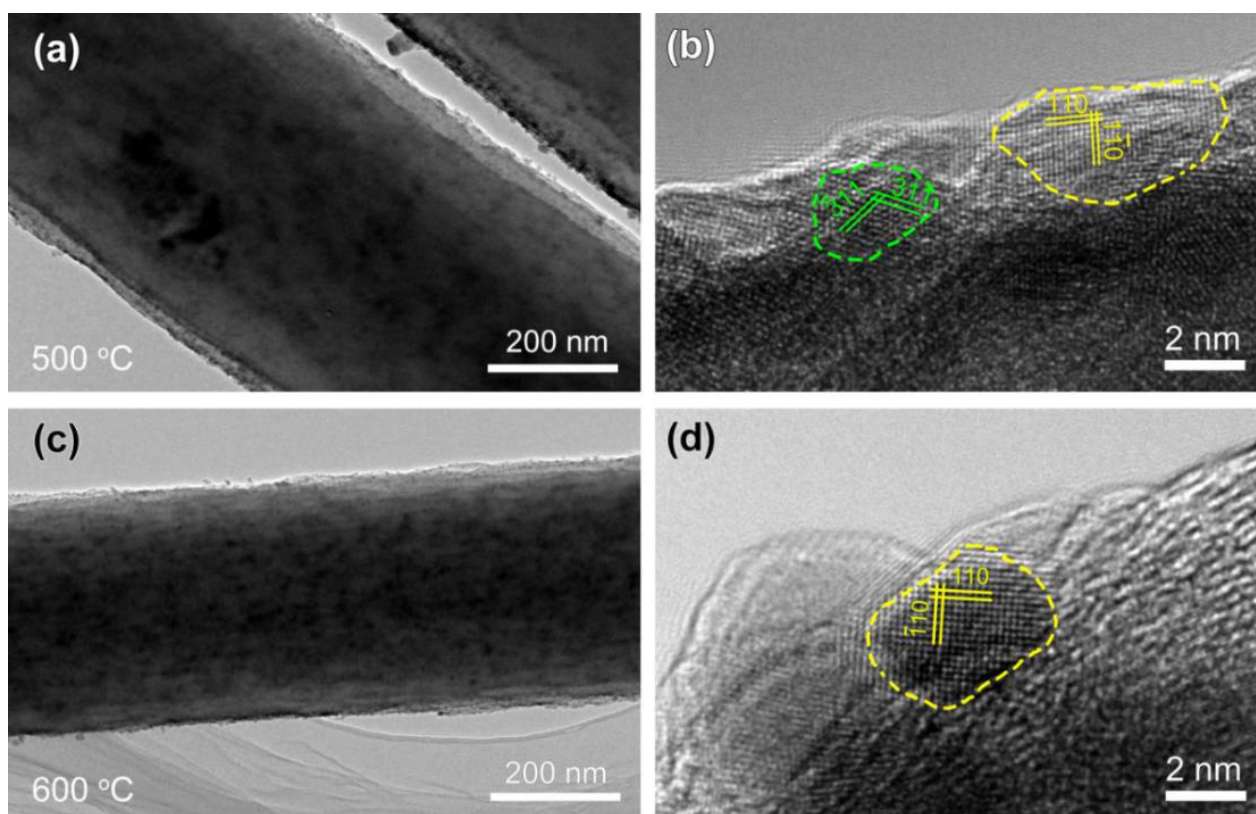


Figure 4. (a,b) and (c,d) are TEM and HRTEM images of CF-P 500 and CF-P 600 samples, respectively.

In order to clarify the annealing reaction mechanism of cobalt acetylacetonate and iron acetylacetonate supported by heterogeneous submicron fibers, thermogravimetry (TG) curves of cobalt acetylacetonate (blue line C) and iron acetylacetonate (red line F) heated to 900 °C in air were analyzed and compared with the mixed annealing curve of cobalt acetylacetonate and iron acetylacetonate, shown in Figure 5. As shown in Figure 6, the thermogravimetric curve F shows that iron acetylacetonate begins to decompose at 176 °C. In the temperature range from 176 °C to 376 °C (point a–d), the weight loss of iron acetylacetonate is mainly due to the reduction of -CH₃ and -CH on the acac ligand and the formation of oxides. After point d, there is no obvious weight loss in the curve, indicating that iron acetylacetonate is finally converted into the stable product Fe₂O₃ after heating in the air. The TG curve C of cobalt acetylacetonate shows that the decomposition of cobalt acetylacetonate begins at 71 °C and oxidation begins to form a stable oxide at 223–370 °C (point c–d). In the temperature range from 71 °C to 370 °C (point a–d), the weight loss of cobalt acetylacetonate is mainly due to the loss of -CH₃ and -CH and the formation of Co₃O₄ due to thermal decomposition. After point d, there is no significant weight loss in the curve, indicating that cobalt acetylacetonate is eventually converted to a stable product after heating in air. The product of cobalt acetylacetonate annealed at 600 °C in air was characterized by XRD, and the final product was Co₃O₄, as shown in Figure 7.

Figure 6 shows the TG curves of PAN fiber membrane (P), C₁₅H₂₁CoO₆ (Co(acac)₂), C₁₅H₂₄FeO₆ (Fe(acac)₃) mixed powder (CF) (molar ratio Fe:Co = 2:1) and C₁₅H₂₁CoO₆ (Co(acac)₂)/C₁₅H₂₄FeO₆ (Fe(acac)₃)/PAN heterogeneous submicron fiber membrane (CF-P) (molar ratio Fe:Co = 2:1). The curve CF is obtained by heating a mixed pharmaceutical powder of cobalt acetone and iron acetone from 25 °C to 900 °C at a temperature rate of 10 °C/min in air. TG curves P and CF-P are the curves obtained when the temperature rises from 25 °C to 230 °C for 2 h at a temperature rate of 10 °C/min in an air atmosphere, and then rises to 900 °C at a temperature rate of 10 °C/min in an N₂ atmosphere.

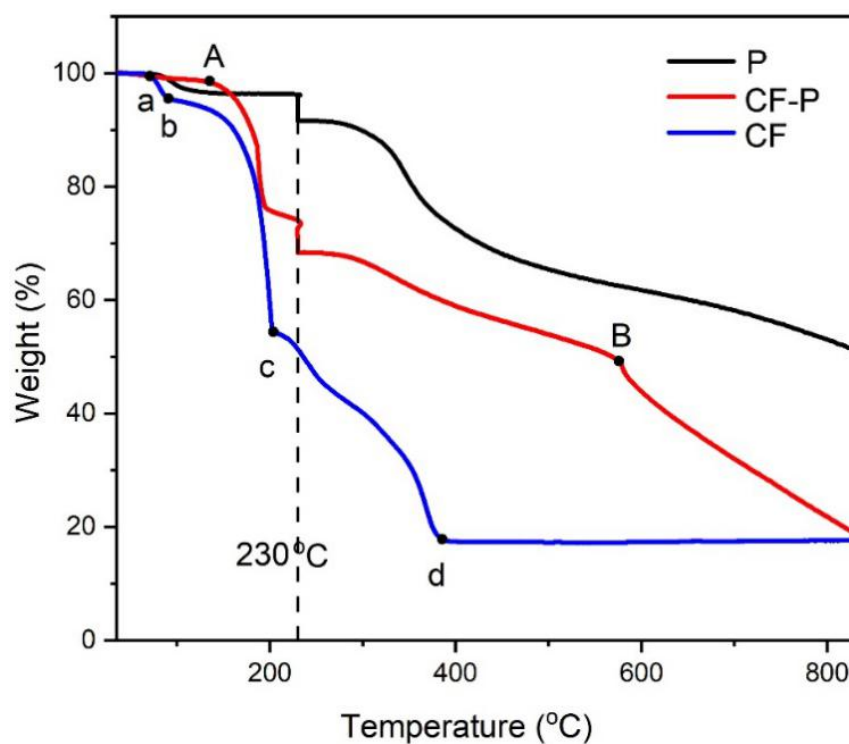


Figure 5. Thermogravimetric curves of PAN fiber membrane (P), $C_{15}H_{21}CoO_6$ ($Co(acac)_2$), $C_{15}H_{24}FeO_6$ ($Fe(acac)_3$) mixed powder (CF) and $C_{15}H_{21}CoO_6$ ($Co(acac)_2$)/ $C_{15}H_{24}FeO_6$ ($Fe(acac)_3$)/PAN heterogeneous submicron fiber membrane (CF-P). In Figure 6, a, b, c and d are the inflection points of the TG curves of $C_{15}H_{21}CoO_6$ ($Co(acac)_2$) and $C_{15}H_{24}FeO_6$ ($Fe(acac)_3$) powder mixtures. A and B are the inflection points of the TG curve of the $C_{15}H_{21}CoO_6$ ($Co(acac)_2$)/ $C_{15}H_{24}FeO_6$ ($Fe(acac)_3$)/PAN heterogeneous submicron fiber membrane.

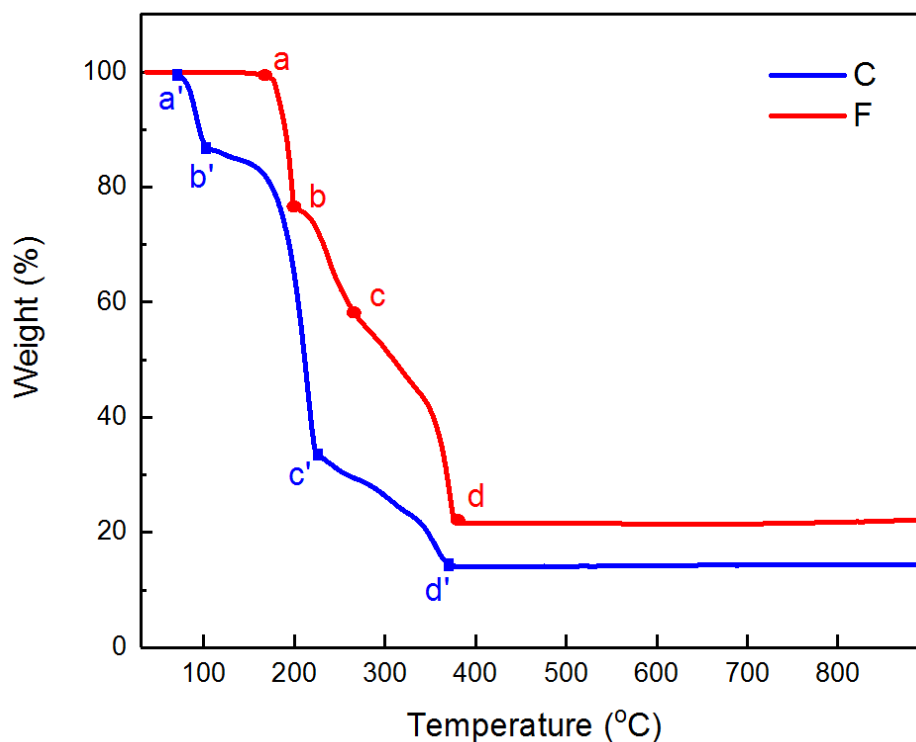


Figure 6. TGA curves of $C_{15}H_{24}FeO_6$ ($Fe(acac)_3$) powder (F) and $C_{15}H_{21}CoO_6$ ($Co(acac)_2$) powder (C) in air.

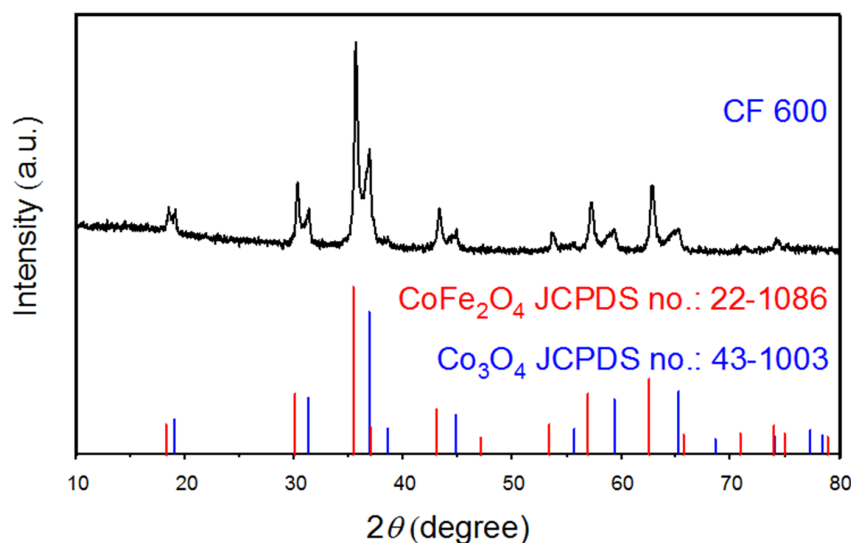
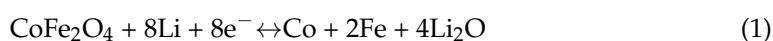


Figure 7. XRD patterns of $C_{15}H_{21}CoO_6$ ($Co(acac)_2$) and $C_{15}H_{24}FeO_6$ ($Fe(acac)_3$) powder mixture (molar ratio Fe:Co = 2:1) after annealing at 600 °C in air.

The TG curve CF-P begins to decline slowly at 138 °C (point A) and at 200 °C there is rapid weight loss, which is due to the thermal decomposition of cobalt acetylacetonate and iron acetylacetonate and the formation of $CoFe_2O_4$ [24]. As the annealing temperature increases further, the cobalt-iron compound is reduced by carbon to form a small portion of cobalt-iron alloy due to the inert gas protection and carbon fiber coating state. When the temperature is 586 °C (point B), a small inflection point of weight loss appears, which is caused by $CoFe_2O_4$ being reduced to cobalt-ferro alloy at this temperature, which is consistent with the XRD pattern in Figure 3. Subsequently, in the range of 600–800 °C, all $CoFe_2O_4$ in the heterogeneous carbon submicron fibers was reduced to cobalt-ferro alloy, while only single-phase cobalt-ferro alloy was loaded in the carbon submicron fibers.

According to the above analysis, the phase transformation mechanism of heterogeneous submicron fibers loaded with cobalt acetylacetonate and acetylacetonate iron start to break down at ~138 °C. When the temperature reaches 200 °C, the binary metal oxide $CoFe_2O_4$ is formed [25]. With the increase in annealing temperature to 230 °C, under the protection of inert gas, the binary metal compound is reduced by a small fraction of carbon in the carbon fiber to cobalt-ferroalloy, and then $CoFe_2O_4$ and cobalt-ferroalloy coexist in the heterogeneous carbon submicron fiber. When the temperature reaches 586 °C, $CoFe_2O_4$ is rapidly reduced to cobalt alloy. Therefore, under 600 °C, 700 °C and 800 °C in the preparation of heterogeneous carbon submicron fiber samples, only cobalt alloy single crystal fibers are loaded.

Carbon submicron fiber self-supporting membrane samples CF-P 500 and CF-P 700 loaded with $CoFe_2O_4$ /CoFe alloy were prepared and used as the negative electrodes of lithium-ion batteries, and their electrochemical properties were tested. Figure 9a shows the voltammetry curves of the first six cycles of CF-P 500. As can be seen from the figure, the cyclic voltammetry (CV) curve has an obvious redox peak. During the first cathode scan, there is a reduction peak at 0.42 V due to the formation of the SEI film, which gradually disappears in subsequent turns. The reduction peak at 1.32 V is due to the reduction of $CoFe_2O_4$ to cobalt and iron. During the first anode scan, the peak at 1.35 V is associated with the oxidation of cobalt and iron to CoO and Fe_2O_3 [26]. In the subsequent scanning process, the CV curves almost overlap, which indicates that the sample CF-P 500 has good reversibility during the charging and discharging process. The corresponding reversible reaction is as follows [27–29]:



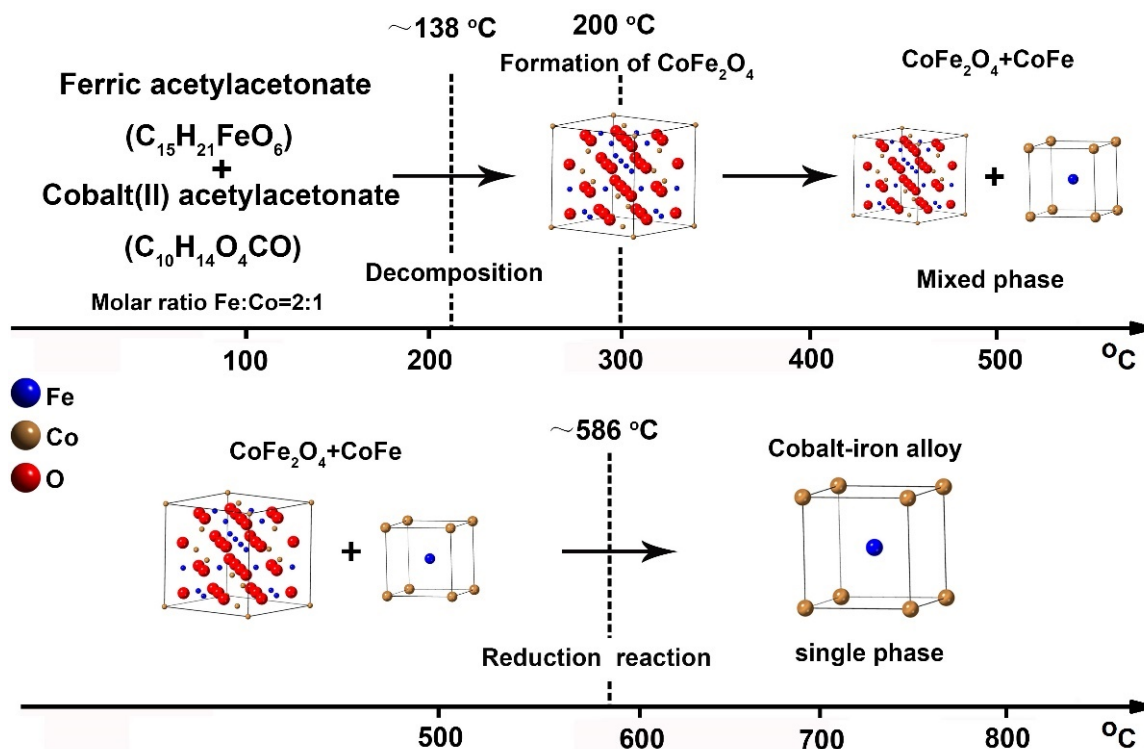


Figure 8. Phase transition of cobalt-Fe-based nanocrystals in carbon submicron fibers with heterogeneous structures.

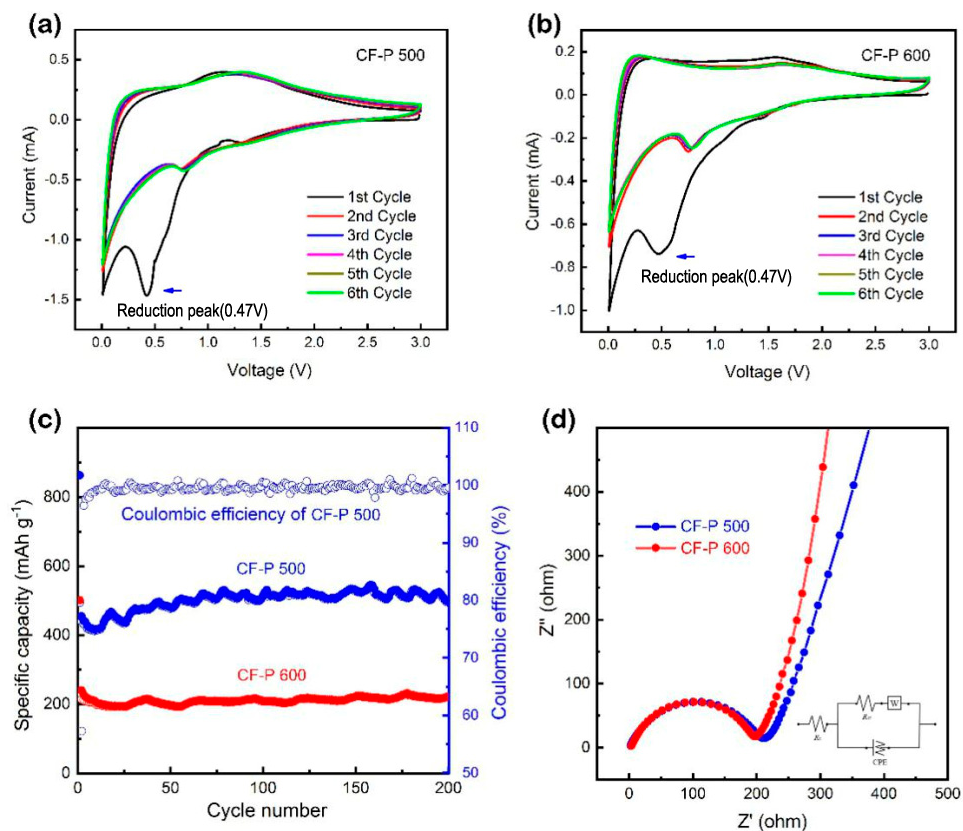


Figure 9. Electrochemical properties of the samples CF-P 500 and CF-P 700: (a,b) cyclic voltammery curves, (c) cyclic properties with a current density of 500 mA g^{-1} and (d) EIS spectra of the electrodes, illustrated with their equivalent circuit diagram.

Figure 9b shows the voltammetry curve of the first six cycles of the sample CF-P700. During the first cycle of cathodic scanning, a significant reduction peak appeared at 0.47 V due to the decomposition of the electrolyte to form the SEI film. After the second cycle, the reduction peak disappeared. In the subsequent scanning process, the shape of the CV curve was similar to that of the negative carbon electrode, indicating that the cobalt-ferro alloy did not have oxidation–reduction properties. As can be seen from the figure, the CV curves from the second to the sixth laps almost coincide, indicating that the redox reaction has good reversibility [30–32].

Figure 9c shows the cyclic performance of CF-P 500 and CF-P 700. As can be seen from the figure, when the current density is 500 mA g^{-1} , both CF-P 500 and CF-P 700 have a good cyclic stability. After 200 cycles, the specific capacity of CF-P 500 is 500 mAhg^{-1} , significantly larger than the specific capacity of CF-P 700. It shows that the specific capacity of the composite carbon submicron fiber electrode material can be significantly improved by the introduction of CoFe_2O_4 . Figure 9d shows the AC impedance spectra of CF-P 500 and CF-P 700. It can be seen from the Figure 10 that the semicircle radius of the impedance curve of CF-P 700 is significantly smaller than that of CF-P 500. After fitting, the RCTS of CF-P 500 and CF-P 700 are 185Ω and 162Ω , respectively. The smaller impedance of the CF-P 700 electrode is due to the high amount of cobalt-ferro alloy in the electrode.

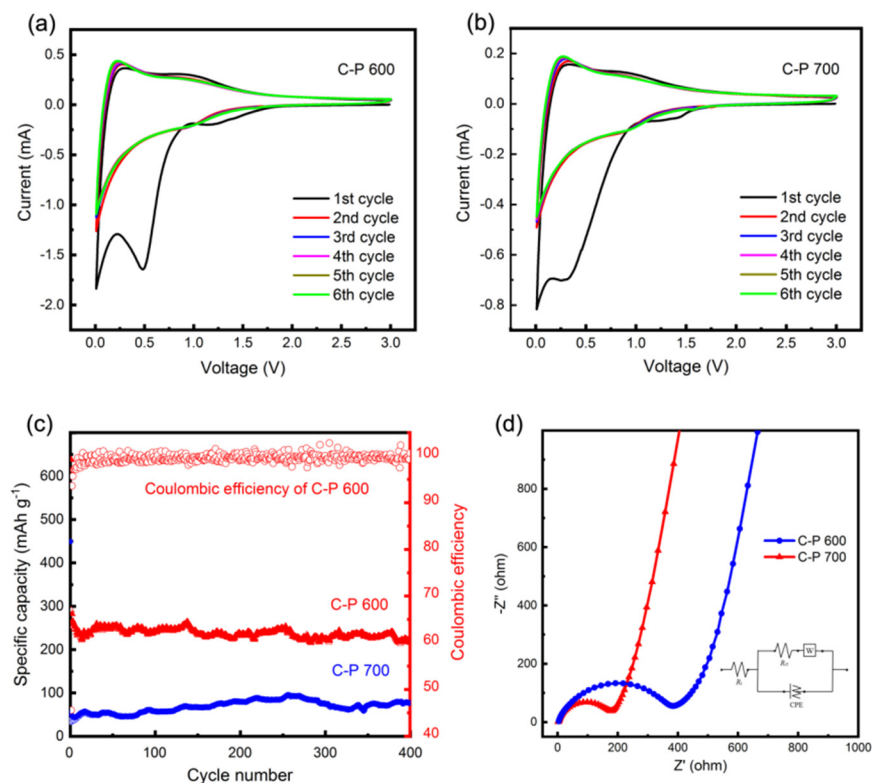


Figure 10. Electrochemical properties of samples C-P 600 and C-P 700: (a,b) cyclic voltammetry curves, (c) cyclic properties with a current density of 500 mA g^{-1} and (d) EIS spectra and equivalent circuits of electrodes [33].

By comparing the cyclic properties of C-P 600 and CF-P 500 in Figures 9c and 10c, it can be found that the specific capacity of CF-P500 is higher than that of C-P600, indicating that the electrochemical performance of composite carbon nanomaterials loaded with binary cobalt iron oxide is better than that of mono-metal cobalt oxide. As electrode materials of lithium-ion batteries, binary metal oxides can be used for alloy/dealloying and conversion reactions at the same time in the process of lithium intercalation. The two reactions form a synergistic effect and have a better lithium storage capacity.

4. Conclusions

Carbon submicron fiber composites loaded with binary metal oxide $\text{CoFe}_2\text{O}_4/\text{CoFe}$ and a cobalt-iron alloy were prepared by electrospinning and high temperature annealing processes. The phase transformation mechanism of the binary metal compounds and alloys in heterogeneous carbon fibers was described. The electrochemical properties of carbon submicron fiber composites loaded with a cobalt-iron alloy and cobalt-iron oxide were studied. The results showed that at 138 °C, the heterogeneous submicron fibers of cobalt acetylacetonate and acetylacetonate iron began to decompose and at ~200 °C, CoFe_2O_4 was generated in the fiber. As the annealing temperature was increased further, some metal compounds in the carbon fiber were reduced to the CoFe_2O_4 alloy, and two phases of CoFe_2O_4 and CoFe-Fe-alloy existed in the fiber. When the temperature reached 586 °C, CoFe_2O_4 was reduced to cobalt alloy, since at 600–800 °C, only the cobalt alloy phase existed in the heterogeneous carbon submicron fiber. Electrochemical performance studies showed that when the binary metal oxides were used as electrode materials for lithium-ion batteries, alloy dealloying and conversion reactions can occur at the same time in the reverse process of lithium intercalation, the two reactions form a synergistic effect, and the cobalt-iron alloy in the material increases the electrical conductivity. Therefore, the carbon submicron fiber loaded with $\text{CoFe}_2\text{O}_4/\text{CoFe}$ has an excellent electrochemical performance.

Author Contributions: Conceptualization, P.X. and N.H.; methodology, W.J. and P.X.; software, Y.S.; validation, Y.Z., Q.Y. and R.Y.; formal analysis, N.H.; investigation, Q.Y.; resources, P.X.; data curation, Q.Y.; writing—original draft preparation, P.X.; writing—review and editing, P.X.; visualization, Y.S.; supervision, P.X. and N.H.; project administration, P.X. and N.H.; funding acquisition, P.X. and N.H. All authors have read and agreed to the published version of the manuscript.

Funding: This research was funded by the Ministry of Education University-Industry Collaborative Education Program (202101326005, 202102295003); 2019, 2020 Innovative Experimental Teaching Project of Qingdao University; Shandong Province Higher Educational Science and Technology Program (J18KB056) and the Binzhou Science and Technology Policy Guidance Program (2022SHFZ012).

Data Availability Statement: Not applicable.

Acknowledgments: Qingdao University Analysis and Testing Center provided the experimental equipment and technical support for this study.

Conflicts of Interest: The authors declare no conflict of interest.

References

1. Li, Y.; Zhang, P.; Guo, Z.; Liu, H.; Yang, J. $\text{NiCo}_2\text{O}_4/\text{C}$ nanocomposite as a highly reversible anode material for lithium-ion batteries. *Electrochim. Solid-State Lett.* **2008**, *11*, A64–A67.
2. Wang, Y.; Park, J.; Sun, B.; Ahn, H.; Wang, G. Wintersweet-flower-like $\text{CoFe}_2\text{O}_4/\text{MWCNTs}$ hybrid material for high-capacity reversible lithium storage. *Chem-Asian J.* **2012**, *7*, 1940–1946. [[CrossRef](#)]
3. Feng, D.Y.; Yang, H.; Guo, X. 3-Dimensional hierarchically porous $\text{ZnFe}_2\text{O}_4/\text{C}$ composites with stable performance as anode materials for Li-ion batteries. *Chem. Eng. J.* **2019**, *355*, 687–696. [[CrossRef](#)]
4. Wang, M.Y.; Huang, Y.; Chen, X.F.; Wang, K.; Wu, H.W.; Zhang, N.; Fu, H.T. Synthesis of nitrogen and sulfur co-doped graphene supported hollow ZnFe_2O_4 nanosphere composites for application in lithium-ion batteries. *J. Alloys Compd.* **2017**, *691*, 407–415. [[CrossRef](#)]
5. Zhang, Y.M.; Pelloccione, C.J.; Brady, A.B.; Guo, H.Y.; Smith, P.F.; Liu, P.; Marschlok, A.C.; Takeuchi, K.J.; Takeuchi, E.S. Probing the Li insertion mechanism of ZnFe_2O_4 in Li-ion batteries: A combined X-ray diffraction, extended X-ray absorption fine structure, and density functional theory study. *Chem. Mater.* **2017**, *29*, 4282–4292. [[CrossRef](#)]
6. Cherian, C.T.; Sundaramurthy, J.; Reddy, M.V.; Suresh, K.P.; Mani, K.; Pliszka, D.; Sow, C.H.; Ramakrishna, S.; Chowdari, B.V. Morphologically robust NiFe_2O_4 nanofibers as high capacity Li-ion battery anode material. *ACS Appl. Mater. Inter.* **2013**, *5*, 9957–9963. [[CrossRef](#)]
7. Gong, C.; Bai, Y.J.; Qi, Y.X.; Lun, N.; Feng, J. Preparation of carbon-coated MgFe_2O_4 with excellent cycling and rate performance. *Electrochim. Acta* **2013**, *90*, 119–127. [[CrossRef](#)]
8. He, J.Y.; Xu, P.L.; Zhou, R.; Li, H.; Zu, H.; Zhang, J.; Qin, Y.; Liu, X.; Wang, F. Combustion Synthesized Electrospun InZnO Nanowires for Ultraviolet Photodetectors. *Adv. Electron. Mater.* **2022**, *8*, 2100997. [[CrossRef](#)]
9. Lavela, P.; Tirado, J.L. CoFe_2O_4 and NiFe_2O_4 synthesized by sol-gel procedures for their use as anode materials for Li ion batteries. *J. Power Sources* **2007**, *172*, 379–387. [[CrossRef](#)]

10. Xu, P.; Ding, C.; Li, Z.; Yu, R.; Cui, H.; Gao, S. Photocatalytic degradation of air pollutant by modified nano titanium oxide (TiO₂) in a fluidized bed photoreactor: Optimizing and kinetic modeling. *Chemosphere* **2023**, *319*, 137995. [[CrossRef](#)]
11. Zhang, G.Q.; Lou, X.W. General solution growth of mesoporous NiCo₂O₄ nanosheets on various conductive substrates as high-performance electrodes for supercapacitors. *Adv. Mater.* **2013**, *25*, 976–979. [[CrossRef](#)] [[PubMed](#)]
12. Liu, B.; Zhang, J.; Wang, X.F.; Chen, G.; Chen, D.; Zhou, C.W.; Shen, G.Z. Hierarchical three-dimensional ZnCo₂O₄ nanowire arrays/carbon cloth anodes for a novel class of high-performance flexible lithium-ion batteries. *Nano Lett.* **2012**, *12*, 3005–3011. [[CrossRef](#)] [[PubMed](#)]
13. Li, J.F.; Xiong, S.L.; Li, X.W.; Qian, Y.T. A facile route to synthesize multiporous MnCo₂O₄ and CoMn₂O₄ spinel quasi-hollow spheres with improved lithium storage properties. *Nanoscale* **2013**, *5*, 2045–2054. [[CrossRef](#)]
14. Kang, W.P.; Tang, Y.B.; Li, W.Y.; Yang, X.; Xue, H.T.; Yang, Q.D.; Lee, C.S. High interfacial storage capability of porous NiMn₂O₄/C hierarchical tremella-like nanostructures as the lithium ion battery anode. *Nanoscale* **2015**, *7*, 225–231. [[CrossRef](#)] [[PubMed](#)]
15. Chen, Y.; Ma, K.; Xu, P.L.; Si, H.Z.; Duan, Y.B.; Zhai, H. Design and Screening of New Lead Compounds for Autism Based on QSAR Model and Molecular Docking Studies. *Molecules* **2022**, *27*, 7285. [[CrossRef](#)]
16. Xu, P.; Cui, L.; Gao, S.; Na, N.; Ebadi, A.G. A theoretical study on sensing properties of in-doped ZnO nanosheet toward acetylene. *Mol. Phys.* **2022**, *120*, e2002957. [[CrossRef](#)]
17. Li, H.; Xu, P.L.; Liu, D.; He, J.Y.; Zu, H.L.; Song, J.J.; Zhang, J.; Tian, F.H.; Yun, M.J.; Wang, F.Y. Low-voltage and fast-response SnO₂ nanotubes/perovskite heterostructure photodetector. *Nanotechnology* **2021**, *32*, 375202. [[CrossRef](#)] [[PubMed](#)]
18. Zhang, L.H.; Hou, L.R.; Lian, L.; Wang, L.S.; Yuan, C.Z. Research progress of Mn-based mixed binary metal oxide anodes for lithium-ion battery. *Rare Metal Mat. Eng.* **2016**, *45*, 1910–1916.
19. Kulkarni, P.; Balkrishna, R.G.; Ghosh, D.; Rawat, R.S.; Medwal, R.; Chowdari, B.V.R.; Karim, Z.; Reddy, M.V. Molten salt synthesis of CoFe₂O₄ and its energy storage properties. *Mater. Chem. Phys.* **2021**, *257*, 123747. [[CrossRef](#)]
20. Xie, W.; Wang, Y.; Zhou, J.; Zhang, M.; Yu, J.L.; Zhu, C.Z.; Xu, J. MOF-derived CoFe₂O₄ nanorods anchored in MXene nanosheets for all pseudocapacitive flexible supercapacitors with superior energy storage. *Appl. Surf. Sci.* **2020**, *534*, 147584. [[CrossRef](#)]
21. Wu, G.; More, K.L.; Johnston, C.M.; Zelenay, P. High-performance electrocatalysts for oxygen reduction derived from polyaniline, iron, and cobalt. *Science* **2011**, *332*, 443–447. [[CrossRef](#)]
22. Ji, C.; Liu, Y.; Li, Y.Y.; Su, X.L.; Xu, J.; Lu, L.L. Facile preparation and excellent microwave absorption properties of cobalt-iron/porous carbon composite materials. *J. Magn. Magn. Mater.* **2021**, *527*, 167776. [[CrossRef](#)]
23. Xu, P.L.; Cao, J.Y.; Yin, C.; Wang, L.T.; Wu, L. Quantum chemical study on the adsorption of megalol drug on the pristine BC₃ nanosheet. *Supramol. Chem.* **2021**, *33*, 63–69. [[CrossRef](#)]
24. Sun, S.; Zeng, H.; Robinson, D.B.; Raoux, S.; Rice, P.M.; Wang, S.X.; Li, G. Monodisperse MFe₂O₄ (M = Fe, Co, Mn) nanoparticles. *J. Am. Chem. Soc.* **2004**, *126*, 273–279. [[CrossRef](#)]
25. Zhong, M.; Yang, D.H.; Kong, L.J.; Shuang, W.; Zhang, Y.H.; Bu, X.H. Bimetallic metal–organic framework derived Co₃O₄-CoFe₂O₄ composites with different Fe/Co molar ratios as anode materials for lithium ion batteries. *Dalton Trans.* **2017**, *46*, 15947–15953. [[CrossRef](#)]
26. Li, T.; Yin, W.; Gao, S.; Sun, Y.; Xu, P.; Wu, S.; Kong, H.; Yang, G.; Wei, G. The Combination of Two-Dimensional Nanomaterials with Metal Oxide Nanoparticles for Gas Sensors: A Review. *Nanomaterials* **2022**, *12*, 982. [[CrossRef](#)]
27. Qi, B.; Gao, S.; Xu, P. The Application of Recycled Epoxy Plastic Sheets Waste to Replace Concrete in Urban Construction and Building. *Processes* **2023**, *11*, 201. [[CrossRef](#)]
28. Xu, P.; Na, N.; Mohamad, A.M. Investigation the application of pristine graphdiyne (GDY) and boron-doped graphdiyne (BGDY) as an electronic sensor for detection of anticancer drug. *Comput. Theor. Chem.* **2020**, *1190*, 112996. [[CrossRef](#)]
29. Li, T.; Shang, D.; Gao, S.; Wang, B.; Kong, H.; Yang, G.; Shu, W.; Xu, P.; Wei, G. Two-Dimensional Material-Based Electrochemical Sensors/Biosensors for Food Safety and Biomolecular Detection. *Biosensors* **2022**, *12*, 314. [[CrossRef](#)] [[PubMed](#)]
30. Geng, C.; Zhao, Z.; Xue, Z.; Xu, P.; Xia, Y. Preparation of Ion-Exchanged TEMPO-Oxidized Celluloses as Flame Retardant Products. *Molecules* **2019**, *24*, 1947. [[CrossRef](#)] [[PubMed](#)]
31. Song, L.; Qiao, X.L.; Sun, J.X.; Yi, N.; Wang, M.Y.; Zhao, Z.H.; Xie, R.Y.; Chen, W.C.; Xia, Y.Z. Wet-spinning fluorescent alginate fibres achieved by doping PEI modified CPDs for multiple anti-counterfeiting. *Carbohydr. Polym.* **2023**, *304*, 120500. [[CrossRef](#)] [[PubMed](#)]
32. Qi, B.; Gao, S.; Xu, P. The Application of Rubber Aggregate-Combined Permeable Concrete Mixture in Sponge City Construction. *Coatings* **2023**, *13*, 87. [[CrossRef](#)]
33. Xu, P.; Yuan, Q.; Ji, W.; Yu, R.; Wang, F.; Huo, N. Study on the controllable preparation, phase transition mechanism and electrochemical properties of carbon submicron fibers loaded with cobalt and compounds. *Mater. Express* **2023**, *12*, in press.

Disclaimer/Publisher’s Note: The statements, opinions and data contained in all publications are solely those of the individual author(s) and contributor(s) and not of MDPI and/or the editor(s). MDPI and/or the editor(s) disclaim responsibility for any injury to people or property resulting from any ideas, methods, instructions or products referred to in the content.